



HAL
open science

Study of plasma etching impact on chemoepitaxy directed self-assembly

Maria Gabriela Gusmão Cacho, Khatia Benotmane, Aurélie Le Penneç,
Charlotte Bouet, Patricia Pimenta-Barros, Guido Rademaker, Maxime
Argoud, Raluca Tiron, Nicolas Possémé

► **To cite this version:**

Maria Gabriela Gusmão Cacho, Khatia Benotmane, Aurélie Le Penneç, Charlotte Bouet, Patricia Pimenta-Barros, et al.. Study of plasma etching impact on chemoepitaxy directed self-assembly. Journal of Vacuum Science & Technology A, 2021, 39 (3), 10.1116/6.0000850 . cea-04951899

HAL Id: cea-04951899

<https://cea.hal.science/cea-04951899v1>

Submitted on 17 Feb 2025





HAL is a multi-disciplinary open access archive for the deposit and dissemination of scientific research documents, whether they are published or not. The documents may come from teaching and research institutions in France or abroad, or from public or private research centers.

L'archive ouverte pluridisciplinaire **HAL**, est destinée au dépôt et à la diffusion de documents scientifiques de niveau recherche, publiés ou non, émanant des établissements d'enseignement et de recherche français ou étrangers, des laboratoires publics ou privés.



RESEARCH ARTICLE | MARCH 29 2021

Study of plasma etching impact on chemoepitaxy directed self-assembly

Maria Gabriela Gusmão Cacho ; Khatia Benotmane; Aurélie Le Pennec; Charlotte Bouet; Patricia Pimenta-Barros; Guido Rademaker ; Maxime Argoud; Raluca Tiron ; Nicolas Possémé 



J. Vac. Sci. Technol. A 39, 033004 (2021)

<https://doi.org/10.1116/6.0000850>



View
Online



Export
Citation

Articles You May Be Interested In

Block copolymer directed self-assembly defect modes induced by localized errors in chemoepitaxial guiding underlayers: A molecular simulation study

J. Vac. Sci. Technol. B (May 2020)

Selective plasma etching of silicon-containing high chi block copolymer for directed self-assembly (DSA) application

J. Vac. Sci. Technol. B (June 2021)

Increase of space width roughness in directed self-assembly patterning arising from shrinking stress in the remaining poly(methyl methacrylate)

J. Vac. Sci. Technol. B (September 2019)



Advance your science and
career as a member of

AVS

LEARN MORE



Study of plasma etching impact on chemoepitaxy directed self-assembly

Cite as: J. Vac. Sci. Technol. A 39, 033004 (2021); doi: 10.1116/6.0000850

Submitted: 9 December 2020 · Accepted: 9 March 2021 ·

Published Online: 29 March 2021



View Online



Export Citation



CrossMark

Maria Gabriela Gusmão Cacho,^{a)} Khatia Benotmane, Aurélie Le Penneç, Charlotte Bouet, Patricia Pimenta-Barros, Guido Rademaker, Maxime Argoud, Raluca Tiron, and Nicolas Possémé

AFFILIATIONS

Technological Platform Department, Univ. Grenoble Alpes, CEA, Leti, F-38000 Grenoble, France

^{a)}Electronic mail: mariagabriela.gusmaocacho@cea.fr

ABSTRACT

Directed self-assembly (DSA) of block copolymers is one of the most promising solutions investigated to obtain small and dense patterns for the sub-10 nm nodes. One of the most important aspects of the DSA technology is the orientation control of the block copolymer, which is determined by surface properties and different guiding techniques. Regarding the Arkema-CEA (ACE) chemoepitaxy process, one of the critical parameters is the preservation of the neutral layer's properties during hydrofluoric acid wet etching, especially regarding its adherence to the titanium nitride (TiN) hard mask. In this paper, the different etching steps involved in the ACE integration flow are evaluated. Their effects on the surface properties of the TiN hard mask and on the adherence of the neutral layer are investigated by x-ray photoelectron spectroscopy and contact angle measurements. Finally, the results obtained are used to optimize the different etching steps, thus demonstrating the chemoepitaxy of a polystyrene-*b*-poly(methyl methacrylate) block copolymer with 32 nm pitch without alignment defects on a 100 μm^2 surface.

Published under license by AVS. <https://doi.org/10.1116/6.0000850>

I. INTRODUCTION

Since Moore's law predicted that the number of transistors in a dense integrated circuit would double every two years,^{1,2} there has been great interest, driven by both economic and performance aspects, to develop technologies that allow the industry to constantly reduce the size of the transistors, thus increasing the number of transistors on the same surface.

Over the last few years, as we approach the sub-10 nm technological nodes, pattern scaling has slowed down due to conventional lithography limitations, mainly in terms of resolution.³ In order to overcome the resolution issue, new patterning techniques, such as extreme ultraviolet lithography, directed self-assembly (DSA), and multiple patterning, have been developed as solutions to continue pattern scaling and to address future node requirements.⁴

This article will focus on the DSA of block copolymers (BCPs) as a low-cost solution to obtain small and dense patterns. This technique is based on the self-assembling property of block copolymers, which are capable of microphase separating, spontaneously forming a dense array of differently ordered nanostructures, like cylinders or lamellae, with domain dimensions of around 5–50 nm. Another advantage is to combine with already available industry

processes, such as 193 nm immersion lithography, therefore meeting manufacturing constraints like cost and equipment availability, among others.³

One of the most important aspects of the DSA is the control of the orientation of the block copolymer. In fact, such orientation is controlled by surface properties, particularly the affinity between the two blocks and the substrate.⁵ For example, for the polystyrene-*b*-poly(methyl methacrylate) (PS-*b*-PMMA) block copolymer with lamellar morphology—the one most used for line/space application because of its well-known properties and synthesis,⁶ if it is deposited directly onto the silicon substrate, the PS block will occupy the interface Si/BCP since it has more affinity to silicon, and the PS-*b*-PMMA block copolymer will therefore organize itself into horizontal lamellae, as illustrated in Fig. 1(a).

In order to obtain the vertical lamellae independently of the substrate's affinity to one of the blocks, a thin polymer layer is deposited on the substrate. This layer is commonly referred to as neutral layer because it has the same affinity for both phases of the block copolymer and thus allows the formation of vertical morphologies,⁵ as illustrated in Fig. 1(b). For the lamellar BCP, Fig. 1(c) shows a top-view scanning electron microscopy (SEM)

17 February 2025 13:02:13

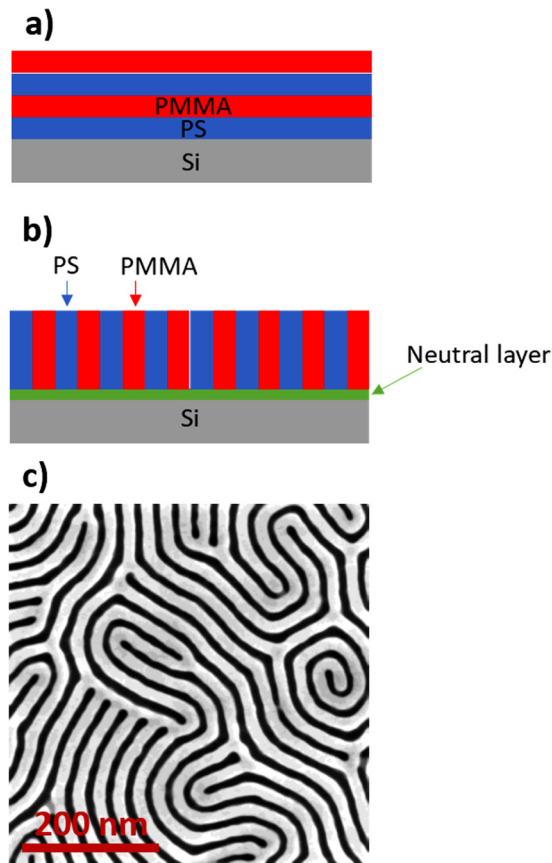


FIG. 1. (a) Schema for the PS-*b*-PMMA deposited directly over the substrate, forming horizontal lamellae; (b) schema for the PS-*b*-PMMA deposited over a neutral layer, thus forming vertical lamellae; (c) top-view SEM image of PS-*b*-PMMA assembled into a fingerprint-like vertical structure thanks to the neutral layer. The PMMA has been removed through dry etching to enhance the contrast.

image of the fingerprint-like structure that is formed once the appropriate neutral layer is used.

The next step in the DSA is to obtain the desired pattern of straight dense lines. For this, two guidance methods have been developed to direct the self-assembly of the block copolymer: graphoepitaxy and chemoepitaxy. These methods consist of synergistically integrating the block copolymer self-assembly with current manufacturing processes, such as 193 nm dry or immersion lithography and spacer patterning, to lead the block copolymers to self-assemble in the desired direction and location by applying chemical or topological constraints.⁷

The graphoepitaxy uses mechanical constraints, such as topographical features obtained by conventional lithography, to act as guide-patterns for the BCP's self-assembly. The BCP is coated and annealed in the space between the guides. For lamellar BCPs, the sidewalls of the guide-patterns preferentially attract one domain of the BCP while the bottom surface is coated with a neutral layer,

allowing lamellar line/space patterns to form parallel to the side-walls of the guide.^{8,9} The graphoepitaxy technique is considered easier to develop, but it presents as disadvantage a lower pattern density, since the topographical features occupy some space on the wafer surface.

The chemoepitaxy, on the other hand, consists of a guiding method by surface property change. Different chemoepitaxy processes have been developed over the last few years, like the LiNe flow¹⁰ and the SMART flow.¹¹ Overall, the goal of the chemoepitaxy technique is to obtain narrow guiding stripes, which present a chemical affinity to one of the BCP blocks, interlaced with wide neutral layer stripes on the substrate surface. This way, when the BCP is coated and annealed over the surface, the guiding stripes will attract one of the blocks and induce the BCP to organize itself in line/space patterns. Even though this technique is considered more challenging, since it includes more steps than the graphoepitaxy, it is preferred due to its higher patterning density.

In this paper, the chemoepitaxy process being studied is the Arkema-CEA (ACE) flow developed by Paquet *et al.*^{12,13} The ACE process uses silicon nitride (SiN) spacers to obtain very thin stripes with a CD of around 13 nm that are later going to be replaced by a graftable guiding layer, which will induce the BCP to self-assemble into vertical straight lines.

We propose to investigate and understand the impact of the different etching steps involved in the ACE flow on the surface properties (composition and surface energy) of the titanium nitride (TiN) hard mask by x-ray photoelectron spectroscopy (XPS) and contact angle measurements. Their effect on the neutral layer adherence during hydrofluoric acid (HF) wet etching is also evaluated through ellipsometry measurements. Then, the results obtained will be used to optimize the different etching steps, thus validating the chemoepitaxy ACE flow for a PS-*b*-PMMA block copolymer of pitch 32 nm without alignment defects on a 100 μm^2 surface.

II. EXPERIMENTAL SETUP

A. ACE chemoepitaxy process flow

Figure 2 presents the complete schema of the ACE flow. The initial stack consists of a 100 nm thermal oxide (SiO₂) layer over which a 15 nm layer of titanium nitride (TiN) hard mask is deposited by physical vapor deposition (PVD). The first part of the process is equivalent to a self-aligned double patterning (SADP) process. 193 nm immersion lithography is performed on a standard trilayer stack, which consists of, from bottom to top: 73 nm of spin-on carbon (SOC), 35 nm of silicon-containing antireflective coating (SiARC), and 100 nm of lithography photoresist. The trilayer stack is plasma etched in order to transfer the lithography patterns into the SiARC and SOC layers and afterward the SiARC is stripped using HF diluted at 1% to conserve only the SOC mandrel. Then, a 26 nm SiN layer is deposited over the SOC mandrel by plasma-enhanced chemical vapor deposition (PECVD) at 320 °C. Next, this SiN layer is anisotropically dry etched in order to form the spacers and the SOC mandrel is removed through plasma etching, forming spacers with approximately 13 nm that will later be replaced by the guide-patterns for the block copolymer's self-assembly.

17 February 2025 13:02:13

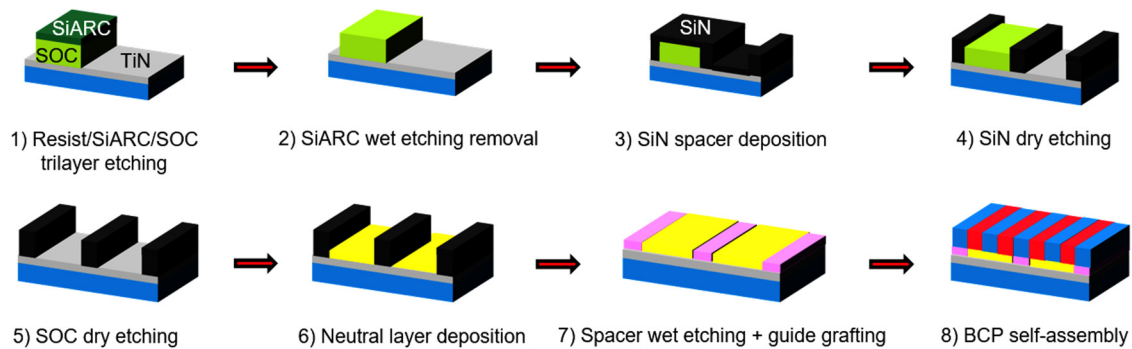


FIG. 2. ACE process flow schema, consisting of a conventional SADP process (steps 1–5), followed by the DSA process (steps 6–8). Reprinted with permission from A. Paquet *et al.*, Proc. SPIE **10958**, 109580M (2019).

The directed self-assembly part of the ACE flow begins by depositing a cross-linkable neutral layer, which will be referred to as “x-NL.” This neutral layer is provided by Brewer Science Inc. and is composed of PS and PMMA. It is deposited by spin-coating in a 300 mm SCREEN SOKUDO Duo™ coat/develop track. It is then annealed at 250 °C for 5 min and rinsed using propylene glycol methyl ether acetate (PGMEA) in the same track, thus filling the area between the spacers to create a neutral surface. Next, the SiN spacers are removed by wet etching using HF diluted at 1%. In the space left by the spacers that were removed, a guiding layer provided by Arkema® is then selectively grafted at 200 °C for 75s, thus obtaining the guiding template for the BCP alignment.

Finally, the block copolymer is spin-coated and annealed to obtain guided line/space patterns. The block copolymer used is a PS-*b*-PMMA provided by Arkema under the trade name Nanostrength® EO with an intrinsic period $L_0 = 32$ nm and a lamellar morphology. The BCP solution is annealed at 240 °C for 15 min to obtain a film with 33 nm thickness.

For the TiN surface study, we use 300 mm silicon blanket wafers with a 30 nm TiN layer deposited by PVD using the same parameters as the ACE flow. The cross-linkable neutral layer (x-NL) used to verify the adherence to the TiN surface is also deposited using the same conditions of the ACE flow: annealing at 250 °C for 5 min followed by a PGMEA rinse.

B. Etching setup

The plasma etching experiments have been carried out on a 300 mm Kiyof FX® inductively coupled plasma (ICP) reactor from LamResearch®, which is powered by an RF generator of 13.56 MHz. As is shown in Fig. 2, the ACE flow presents three plasma etching steps: step 1 corresponds to the conventional trilayer etching, which consists of the pattern transfer of the lithographic photoresist into the SiARC/SOC stack. Step 4 corresponds to the SiN etching to form the spacers. Finally, step 5 represents the SOC mandrel removal once the SiN spacers have been formed. These plasma etching steps are first conducted using well-known plasmas and the parameters can be found in Table I. For the trilayer etching, only the last step, corresponding to the SOC opening, is investigated,

since it is the only one that affects the TiN surface. As we can see in Table I, the SOC opening step (1) presents a short main etch consisting of SO₂/O₂/He followed by an SO₂/He overetch.

The SiARC stripping and the spacer’s wet etching are conducted on a Raider tool from Semitool®. Inside this tool, the wafer is turned over and the etching is done by spraying the wafer with HF droplets diluted in water to obtain the desired concentration of 1%. Once the defined etching time ends, the wafer is again turned over, then dried by isopropanol and N₂ vapor. The respective times used for SiARC stripping and spacer removal are 15 and 60s.

C. Characterization setup

Thickness measurements obtained by ellipsometry before and after the HF wet etching are used to determine the x-NL consumption. The tool used is the Atlas XP+™ from Nanometrics® with an incident angle of 65°. A Cauchy transparent model is used for the thickness measurement from wavelengths between 500 and 1000 nm since this material exhibits no absorption ($k = 0$) in this wavelength range.

Ex situ XPS analysis is conducted to investigate the TiN surface after etching. A Thermo Fisher Scientific® Theta 300™ spectrometer with a monochromatic Al K α x-ray source ($h\nu = 1486.6$ eV) and a spot size of 400 μ m is used. The concentrations of carbon, oxygen, nitrogen, fluor, titanium, sulfur, and chlorine atoms are extracted from the C1s, O1s, N1s, F1s, Ti2p, S2p,

TABLE I. Plasma parameters for the different dry etching steps. The etching times correspond to approximately 50% overetch.

| Step | Chemistry | Pressure (mTorr) | Power (W) | Bias (V) | Flow (ratio) | Time (s) |
|---------------------|---|------------------|-----------|----------|--------------|----------|
| 1: Trilayer etching | ME: SO ₂ /O ₂ /He | 10 | 950 | −250 | 3:0.6:1 | 8 |
| | OE: SO ₂ /He | 10 | 950 | −250 | 3:1 | 17 |
| 4: SiN etching | CH ₂ F ₂ /CF ₄ /O ₂ | 15 | 500 | −400 | 3:1.5:1 | 25 |
| 5: SOC etching | SO ₂ /O ₂ /He | 10 | 950 | −250 | 3:0.6:1 | 25 |

17 February 2025 13:02:13

and Cl2p core-level energy regions, respectively. Binding energies in all XPS spectra are calibrated using the C1s C–C peak (285 eV). All peaks are deconvoluted by a fitting routine consisting of a combination of Lorentzian and Gaussian functions using the Advantage™ software. Each element concentration is obtained by dividing the calculated peak areas by the corresponding Scofield cross section (O1s: 2.88; C1s: 1.0; N1s 1.68; F1s 4.12; Ti2p_{3/2} 4.42; Ti2p_{1/2} 2.06; S2p_{3/2} 1.25; S2p_{1/2} 0.64; Cl2p_{3/2} 1.78; Cl2p_{1/2} 0.96). The sum of the concentrations for the different elements on the analyzed surfaces is equal to 100%. For each element, the measurements consisted of five scans with a dwell time of 500 ms, a pass energy of 100 eV, and an energy step size of 0.1 eV.

Contact angle measurements are conducted to obtain the surface energy of the TiN samples before and after etching. The tool used is the drop shape analyzer DSA100 from Krüss with three different liquids: water, ethylene glycol, and diiodomethane. For each liquid, 10 drops are deposited with the respective volume and flow: water 2 μ l and 3 μ l/s; ethylene glycol 3 μ l and 4 μ l/s; diiodomethane 1.5 μ l and 2 μ l/s. The surface energy and its polar and dispersive components are calculated by the Krüss software using the OWRK (Owens, Wendt, Rabel, and Kaelble)¹⁴ method.

Two types of SEM are used for morphological observations. The critical dimension SEM (CD-SEM) used for top-view observation is the VeritySEM 6i™ tool from Applied Materials®. SEM images are acquired with an accelerating voltage of 800 V and a probe current of 10 pA. After top-view observations, a cross-sectional SEM is performed to observe the TiN and neutral layer surfaces. The tool used is a Hitachi® S5500™ microscope. All images are acquired with an accelerating voltage of 5.0 kV, a probe current of 15 μ A, and using a tilt of -20° .

III. RESULTS AND DISCUSSION

A. Chemoepitaxy results for the nonoptimized ACE flow

The ACE flow described earlier is applied to a 300 mm wafer. Figure 3 represents the top-view SEM image obtained after the BCP self-assembly step for the PS-*b*-PMMA block copolymer with 32 nm pitch. The PMMA phase is removed through dry etching to enhance the contrast and facilitate the image capture. Different types of defects can be seen in this image, like dark spots and BCP alignment defects, which are probably caused by the lift-off of the neutral layer.

These results indicate that the surface properties of the TiN hard mask are modified during different etching steps and, therefore, become less favorable to the wetting and adherence of the neutral layer. The objective of this article is to study the impact of each etching step on the TiN surface and identify the ones that mostly affect its properties, especially regarding its composition and surface energy.

B. Effect of the sequence of etching and deposition steps on the TiN surface

In order to understand the origin of the different defects presented in Fig. 3, the effect of the sequence of etching and deposition steps on the TiN surface is investigated using TiN blanket

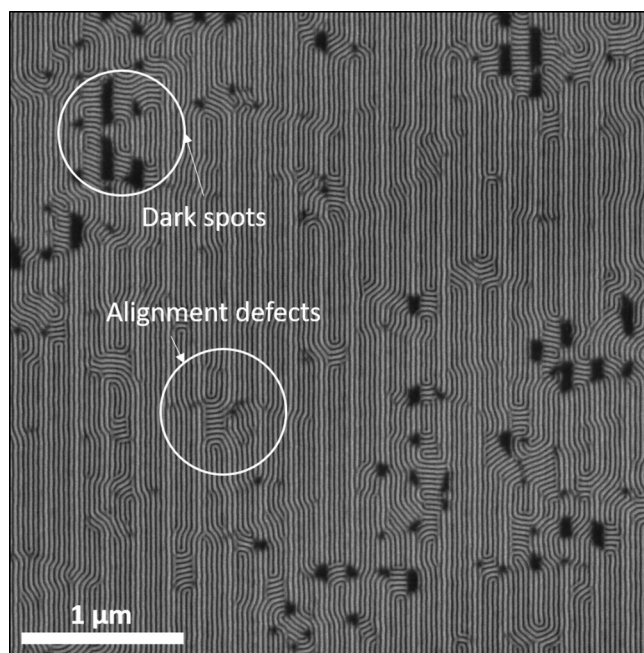
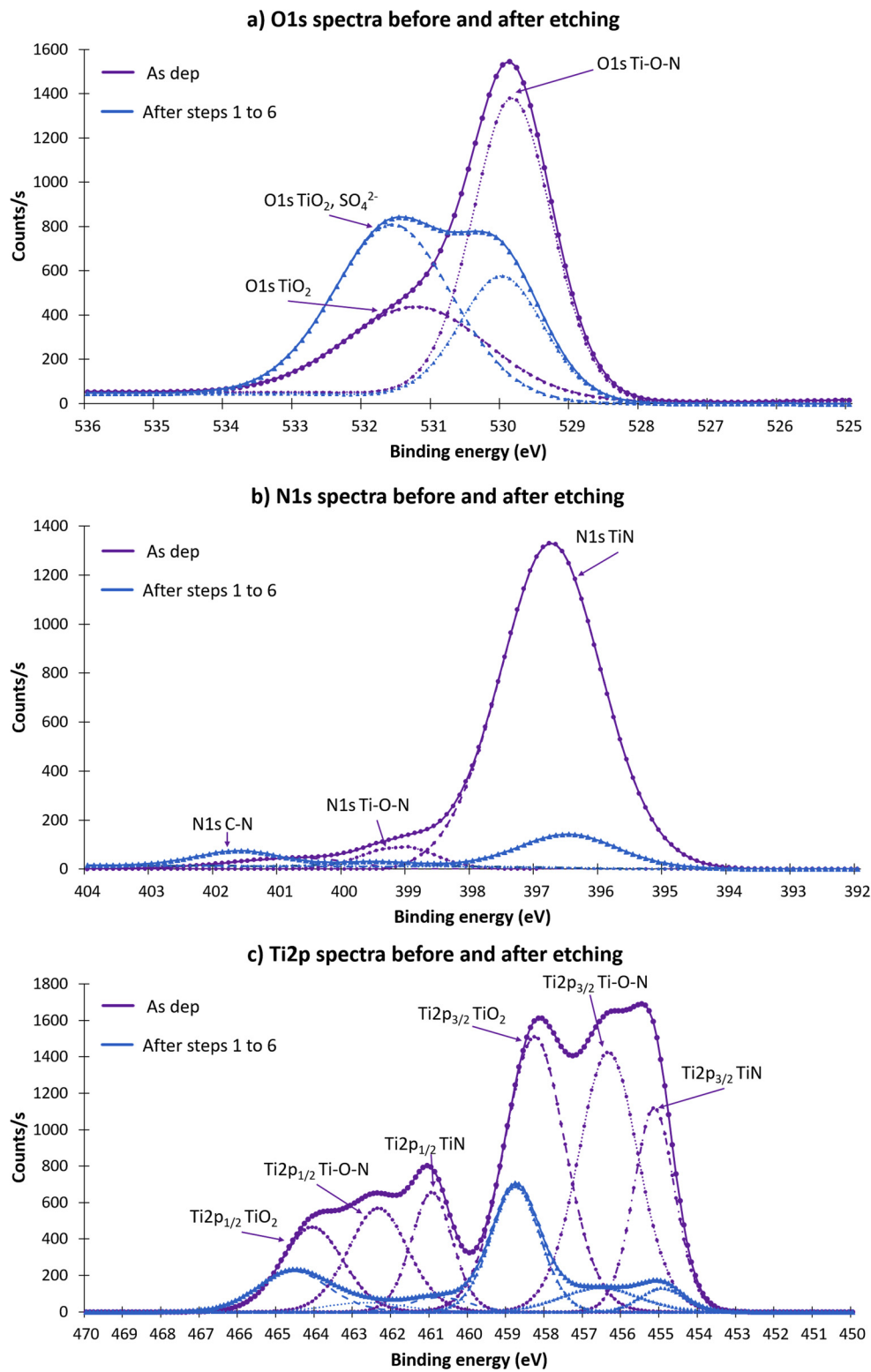


FIG. 3. Top-view SEM image of the PS-*b*-PMMA block copolymer with 32 nm pitch partially aligned by the ACE flow, highlighting the alignment defects and dark spots probably caused by lift-off of the neutral layer.

wafers with a 73 nm SOC layer deposited on top. The trilayer etching and the SiARC stripping are conducted using the parameters presented in Sec. II B. The complete removal of the SOC layer is confirmed by ellipsometry. Then, a 26 nm SiN layer is deposited through PECVD as described in Sec. II A. Next, the SiN and SOC plasma etching are performed using the parameters from Table I. Once again, ellipsometry is used to confirm the complete removal of the SiN layer. Finally, the TiN surface composition and energy are determined by *ex situ* XPS and contact angle measurements, respectively.

1. Study of etching steps impact on TiN surface composition

Figure 4 presents the evolution of O1s (a), N1s (b), and Ti2p (c) *ex situ* XPS spectra for the TiN surface before and after the sequence of etching and deposition (steps 1–5), while Fig. 5 presents the atomic percentage of each element before (a) and after steps 1–5 (b). Figure 4 shows that the TiN surface after steps 1–5 presents a strong oxidation when compared to the as deposited TiN surface, with the increase in TiO₂ (Ti2p_{3/2} peak at around 458.7 eV and O1s peak at 531.6 eV¹⁵) and decrease in TiN (Ti2p_{3/2} peak at around 454.7 eV and N1s peak at 396.9 eV¹⁶) and Ti–O–N (Ti2p_{3/2} peak at around 456.3 eV, N1s peak at 399.6 eV, and O1s peak at 530 eV¹⁶) peaks. Figure 5 indicates that the TiN surface also presents around 13% of sulfur after steps 1–5, represented by TiO_xS_y and SO₄²⁻ with S2p_{3/2} peaks at 163.4 (Ref. 15) and 169.2 eV



17 February 2025 13:02:13

FIG. 4. (a) O1s, (b) N1s, and (c) Ti2p *ex situ* XPS spectra for the TiN surface before and after the sequence of etching and deposition steps 1–5 present on the ACE flow.

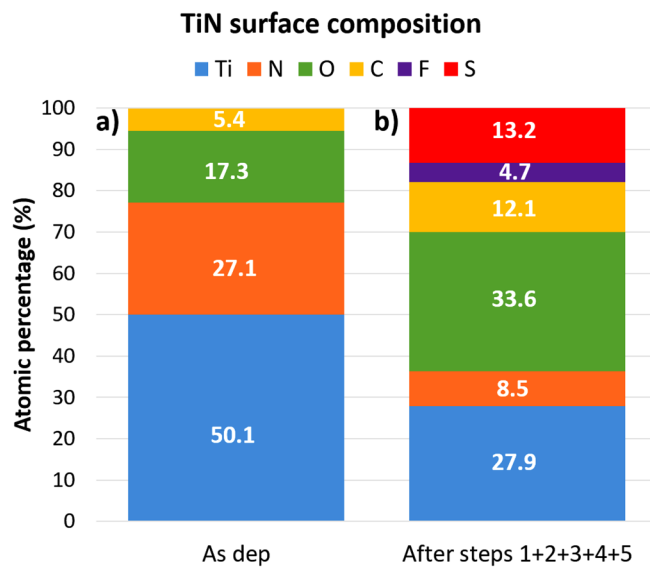


FIG. 5. TiN surface composition determined by *ex situ* XPS (a) before and (b) after the sequence of etching and deposition steps 1–5 present on the ACE flow.

(Ref. 17), respectively. Furthermore, the corresponding O1s peak in Fig. 4(a) also confirmed the presence of SO_4^{2-} . The presence of fluorine is probably due to the SiN etching step, while the presence of carbon is due to contamination from the reactor walls and to the air exposure between the etching and XPS analysis.

2. Contact angle and surface energy measurements

Contact angle measurements are performed on the TiN surface before and after the sequence of etching and deposition steps. The results for the surface energy γ and its dispersive (γ_d) and polar (γ_p) components are summarized in Table II. The sum of γ_d and γ_p corresponds to γ . Previous studies have shown that the surface energy's polar component is the one that best indicates the surface affinity between the neutral layer and the substrate.⁵ These studies show that a substrate with a polar component close to 5 mN/m is attractive to the PS-*r*-PMMA, which composes the neutral layer used for the ACE process.

TABLE II. TiN surface energy before and after the sequence of etching and deposition steps 1–5, calculated by contact angle measurements, as well as its dispersive and polar components.

| Step | Surface energy γ (mN/m) | Dispersive component γ_d (mN/m) | Polar component γ_p (mN/m) |
|------------------|--------------------------------|--|-----------------------------------|
| As deposited TiN | 43.8 | 37.3 | 6.5 |
| After steps 1–5 | 78.3 | 44.8 | 33.5 |

Therefore, it is important to observe that the sequence of etching and deposition steps presented in Table II induces a significant increase in the surface energy's polar component, which goes from 6.5 mN/m for the pristine TiN to approximately 33.5 mN/m for the TiN after steps 1–5. At first glance, this means that the TiN surface is probably not favorable to the wetting of the neutral layer after the sequence of etching and deposition steps.

3. Effect of the wet spacer removal step on the neutral layer adherence

Following the ACE process flow, the next two steps after SOC etching are the neutral layer deposition (step 6) and spacer removal through HF wet etching (step 7). The neutral layer resistance to the HF wet etching is one of the most important parameters that must be verified in order for the ACE process to work. Failure to conserve the neutral layer after wet etching might induce various types of self-assembly defects of the block copolymer, such as the ones presented in Fig. 3.

Therefore, the goal is to verify the adherence of the neutral layer over the TiN surface modified by the sequence of etching and deposition steps. When the substrate presents the adequate surface conditions, the neutral layer adheres to the substrate and cannot be removed through HF dip. For this study, the x-NL neutral layer is deposited over the TiN hard mask after steps 1–5, using the conditions described in Sec. II A. The neutral layer thickness after deposition is measured by ellipsometry. Finally, the 300 mm wafers are submitted to the HF dip with a 1% dilution using two different times in order to evaluate their impact: 15 and 60s. The neutral layer thickness after HF dip is once again measured by ellipsometry.

Table III presents the results obtained for the neutral layer thickness before and after HF wet etching for both the pristine TiN surface and the surface after steps 1–5 in order to be able to compare. For the pristine TiN surface, Table III shows that the neutral layer thickness is the same before and after HF dip, regardless of its duration, which means that the surface state of the pristine TiN is favorable to the adherence of the neutral layer and allows the vertical alignment of the block copolymer during step 8. As was shown in Table II, the pristine TiN surface presents a polar component of 6.5 mN/m. Therefore, this confirms what has been observed in previous studies⁵ and was presented in Sec. III B 2: a substrate with a polar component close to 5 mN/m is attractive to the PS-*r*-PMMA, which composes the neutral layer.

Regarding the TiN surface after the sequence of etching and deposition steps 1–5, Table III shows that the neutral layer

TABLE III. Neutral layer thickness measured by ellipsometry before and after HF dip when deposited over a pristine TiN surface and over the TiN surface after steps 1–5.

| Neutral layer thickness (nm) | Before HF | After HF for 15 s | After HF for 60 s |
|------------------------------|-----------|-------------------|-------------------|
| Pristine TiN | 7.0 ± 0.3 | 7.0 ± 0.3 | 7.0 ± 0.3 |
| TiN after steps 1–5 | 8.9 ± 1.0 | 6.5 ± 1.2 | 0.0 ± 0.0 |

thickness is reduced from 8.9 to 6.5 nm after HF dip for 15s, meaning the x-NL was partially removed during the wet etching. It also shows that after the longer HF dip of 60 s the x-NL was completely removed, with its thickness reduced to zero. Figure 6 presents a cross-sectional SEM image of the surface after HF dip for 15 and 60s. After 15s, neutral layer lift-off spots are visible, while after 60 s these spots are no longer visible due to the x-NL being completely removed. These results indicate that the TiN surface after the sequence of etching and deposition steps present in the ACE process is not favorable to the neutral layer's adherence and, as a result, the neutral layer is removed through a lift-off process when exposed to an HF dip. Therefore, the TiN blanket wafers present the same problems observed for the chemoepitaxy patterned wafers in Sec. III A, meaning this sequence of etching steps is not adapted for the ACE integration flow.

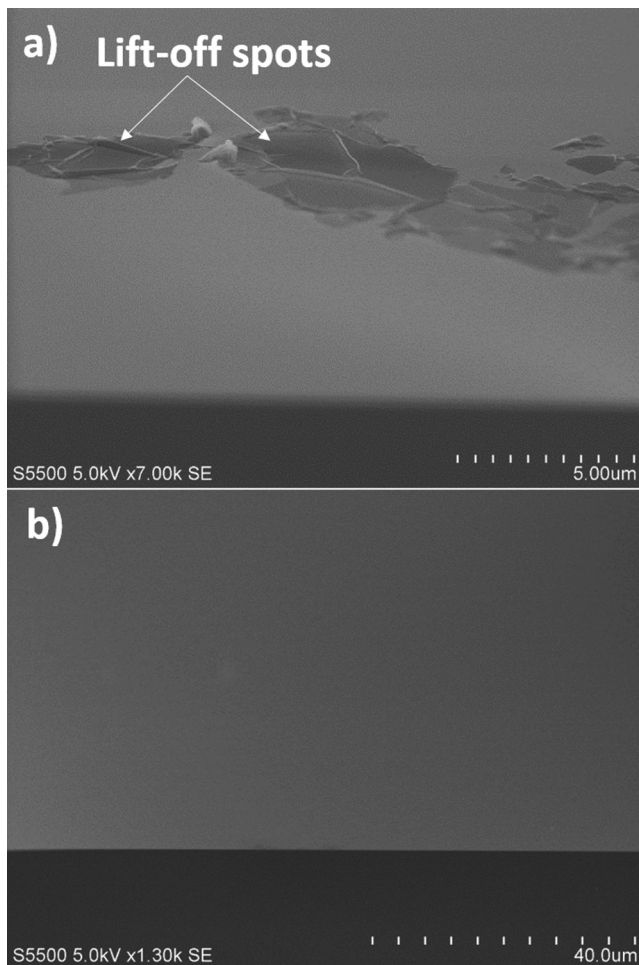


FIG. 6. Cross-sectional SEM image of the TiN + xNL surface after steps 1–5, neutral layer deposition and HF wet etching, indicating (a) the neutral layer lift-off spots after HF dip for 15s and (b) the TiN surface after complete x-NL removal using 60s of HF dip.

C. Effect of each etching step on the TiN surface

In order to identify which etching step is not adequate for the ACE flow integration, the TiN blanket wafers have been exposed to each etching step, taken separately: trilayer dry etching (step 1), SiARC removal by HF wet etching (step 2), SiN spacer dry etching (step 4), and SOC dry etching (step 5). Section II B already presents the chemistries and parameters used for each etching step.

1. Effect of each etching step on the TiN surface composition

Figure 7 presents the *ex situ* XPS results obtained for the TiN surface before and after each etching step. Figures 7(b) and 7(e) show that the trilayer and the SOC etching present a similar result to the one presented in Figs. 4 and 5 after the sequence of steps 1–5: strong increase in the oxygen percentage and a decrease in the nitrogen percentage when compared to the pristine TiN surface [Fig. 7(a)], characterized by the increase in TiO₂ and a decrease in TiN and Ti–O–N bonds. They also present a considerable amount of sulfur, represented by TiO_xS_y, TiOSO₄, and a new S2p_{3/2} peak at 167.2 eV, which might correspond to SO₂.¹⁸ Together, they represent around 12%–15% of the TiN surface. As shown before, the presence of carbon and fluorine is due to contamination from the reactor walls and to the air exposure between the etching and XPS analysis.

Figure 7 also shows the XPS results after wet etching with HF dip and after SiN spacer etching with CH₂F₂/CF₄/O₂. The surface composition after HF presented in Fig. 7(c) is quite similar to that of the pristine TiN, with only a very small amount of fluorine present, represented by an F1s peak at around 684.8 eV, characteristic of metal fluorides, such as TiF_x. Finally, after SiN spacer etching, Fig. 7(d) shows that it presents a small decrease of around 3%–7% each for Ti, N, and O percentages, which is proportional to the considerable amount of fluorine (13.5%) present in this sample and consisting of TiF_x.

2. Contact angle and surface energy measurements

Like in Sec. III B 2, contact angle measurements are conducted on the TiN surface before and after each etching step. The results for the surface energy γ and its dispersive (γ_d) and polar (γ_p) components are presented in Table IV. The results are once again similar to the ones observed in Table II for the sequence of steps 1–5: every etching step induces a significant increase in the surface energy's polar component. The only exception is the SiN etching, which presents a smaller polar component compared to the other etching steps, but still three times higher than that of pristine TiN. This means that the surface energy measurements are not conclusive enough to indicate which etching steps are not adequate for the ACE integration.

Furthermore, the effects of the annealing and PGMEA rinsing steps present on the neutral layer deposition (step 6 of the ACE flow) have also been investigated. The XPS and contact angle results showed that these steps do not influence the TiN surface's composition and energy. For the rest of this study, the focus will remain only on the etching steps.

17 February 2025 13:02:13

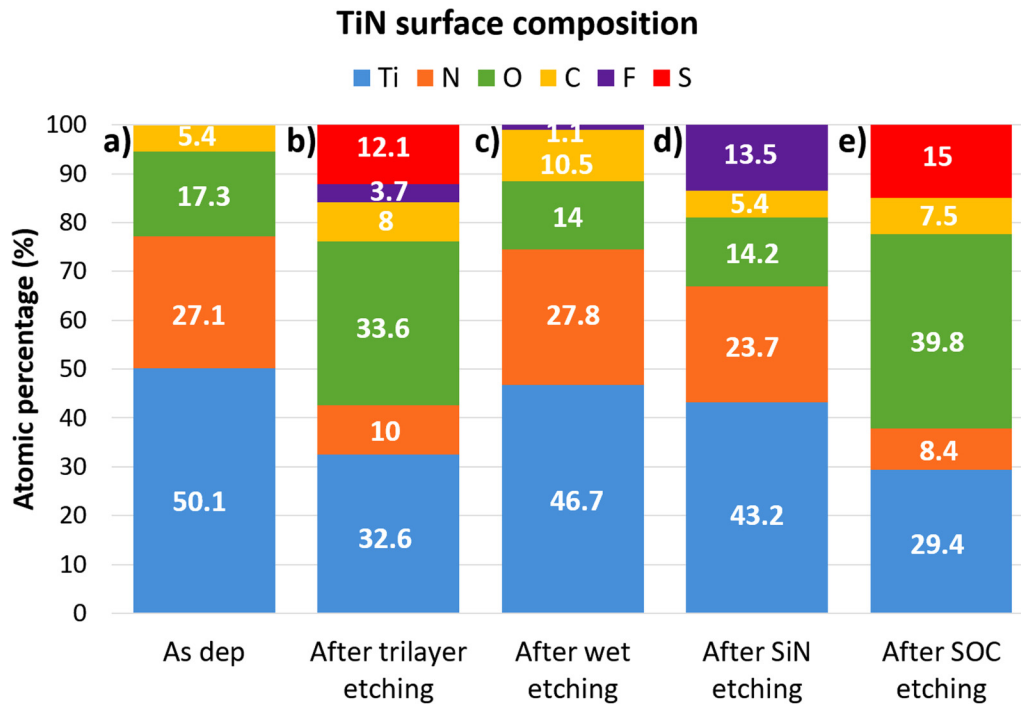


FIG. 7. TiN surface composition determined by *ex situ* XPS before and after each etching step present on the ACE flow: (a) before etching; (b) after trilayer etching; (c) after SiARC wet etching; (d) after SiN etching; and (e) after SOC etching.

3. Effect of the wet spacer removal step on the neutral layer adherence

As described in Sec. III B 3, the neutral layer is deposited over the TiN surface after each etching step and then submitted to an HF wet etching during 60 s in order to evaluate the TiN surface's compatibility to it. The neutral layer thickness is measured before and after HF for each case. The results are presented in Table V.

First, it is important to notice that the trilayer and the SOC etching, which are both based on SO₂/O₂/He plasma, are the only steps that present a complete removal of the neutral layer after HF wet etching. While for the SiARC wet removal by HF and the SiN etching using a fluorocarbon-based recipe, Table V shows that

these steps present the same neutral layer thickness before and after HF etching.

Therefore, based on the different results obtained, the neutral layer lift-off defects observed after the sequence of etching and deposition steps on both patterned and blanket wafers are most probably caused by the interaction of the SO₂/O₂/He plasma with the TiN surface.

D. Understanding the effect of the SO₂/O₂/He etching on the TiN surface and neutral layer deposition

In order to understand the effect of the SO₂/O₂/He plasma on the TiN surface, each gas is applied separately to the TiN blanket wafers, using the same plasma parameters presented in Table I. Furthermore, the effect of ion bombardment has also been investigated by applying the SO₂/O₂/He plasma with zero RF bias power and keeping the other parameters constant.

TABLE IV. TiN surface energy after each etching step, calculated by contact angle measurements, as well as its dispersive and polar components.

| Step | Surface energy γ (mN/m) | Dispersive component γ_d (mN/m) | Polar component γ_p (mN/m) |
|----------------------|--------------------------------|--|-----------------------------------|
| As deposited TiN | 43.8 | 37.3 | 6.5 |
| 1: Trilayer etching | 77.4 | 42.8 | 34.6 |
| 2: SiARC wet etching | 77.0 | 46.0 | 31.0 |
| 4: SiN etching | 57.2 | 36.8 | 20.4 |
| 5: SOC etching | 77.3 | 43.1 | 34.2 |

TABLE V. Neutral layer thickness measured by ellipsometry before and after HF wet etching when deposited over the TiN surface after each etching step.

| Neutral layer thickness (nm) | Before HF | After HF |
|------------------------------|-----------|-----------|
| TiN after trilayer etching | 6.8 ± 0.4 | 0.0 ± 0.0 |
| TiN after SiARC wet etching | 5.8 ± 0.2 | 5.8 ± 0.2 |
| TiN after SiN etching | 5.9 ± 0.3 | 5.9 ± 0.3 |
| TiN after SOC etching | 7.1 ± 0.4 | 0.0 ± 0.0 |

17 February 2025 13:02:13

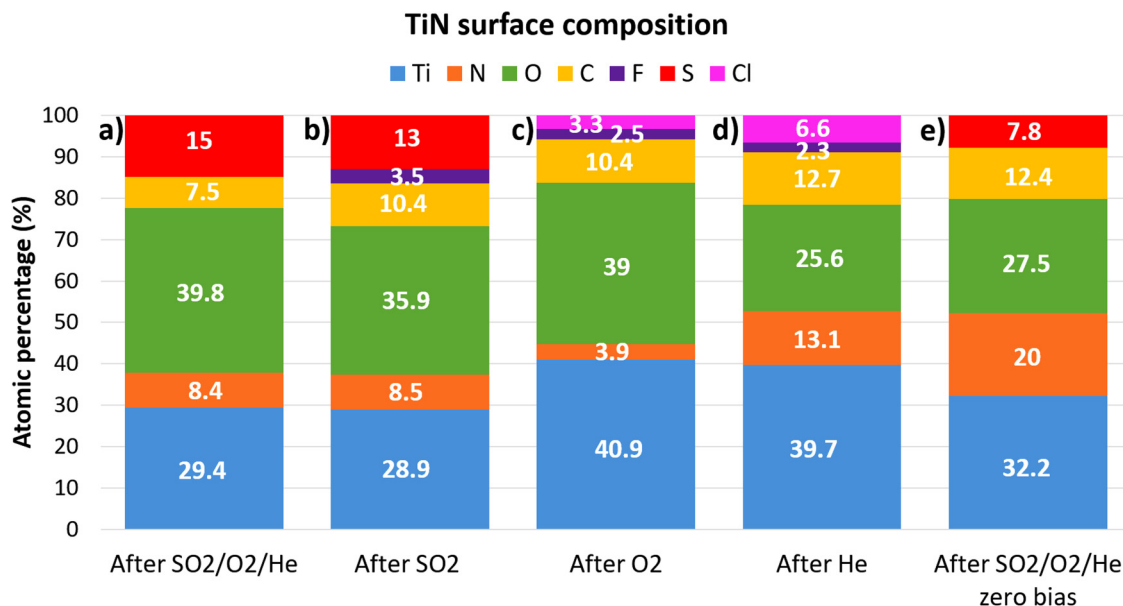


FIG. 8. TiN surface composition determined by *ex situ* XPS: (a) after SO₂/O₂/He (reference); (b) after SO₂ only; (c) after O₂ only; (d) after He only; and (e) after SO₂/O₂/He without RF bias power.

1. Effect of each gas on the TiN surface composition

The XPS results for the TiN surface are presented in Fig. 8. First, when comparing the SO₂/O₂/He results with the results for each gas, the following is observed: for the SO₂ only [Fig. 8(b)], the Ti and N percentages are similar to the reference [Fig. 8(a)], while the oxygen content sees a decrease of about 4%, which is characterized by a slight reduction of the TiO₂ peak. The sulfur percentage is also slightly lower and the SO₂ peak at 167.2 eV is no longer present. As for the O₂ only, Fig. 8(c) shows a significant increase in the titanium percentage due to the increase in the TiO₂ peak intensity. There is also an important reduction of the nitrogen percentage, which is represented by the decrease in the TiN peak intensity. Finally, for the He only [Fig. 8(d)], there is an increase in both Ti and N percentages, characterized by an augmentation of the TiN and Ti–O–N peaks intensity. It is also possible to observe a decrease in the oxygen percentage, a consequence of the decrease in the TiO₂ peak intensity. As expected, sulfur is no longer present on the TiN surface after O₂ only and He only. For all conditions, the carbon, fluorine, and chlorine contamination comes from the etching reactor walls.

Figure 8(e) presents the results after etching using SO₂/O₂/He without RF bias power. When compared to the results with RF bias [Fig. 8(a)], several changes can be noticed: the nitrogen content is increased by about 11.6% compared to the same chemistry with bias, which is characterized by an increase in the TiN peak. A significant decrease in the oxygen percentage of at least 12% is also observed, a consequence of the decrease in the TiO₂ peak intensity. Moreover, it shows a slight increase in the Ti percentage, which is a combination of the TiN peak intensity augmentation and the TiO₂

peak intensity reduction. Finally, a sulfur percentage decrease of 7% is observed and the TiO_xS_y and SO₂ peaks are no longer present. This means that, for the zero bias etching, the thickness of the TiN layer modified by the etching is smaller compared to that of the reference SO₂/O₂/He etching process.

Contact angle measurements have also been conducted for these samples. However, the surface energy values obtained follow the tendency already observed in Sec. III C 2 for the SO₂/O₂/He plasma, with polar component values around 30 mN/m. Therefore, these measures are not conclusive enough for understanding the effect of each gas on the TiN surface and neutral layer adherence.

2. Effect of the wet spacer removal step on the neutral layer adherence

Finally, in order to verify the adherence of the neutral layer over the TiN surface for the different conditions investigated, the

TABLE VI. Neutral layer thickness measured by ellipsometry before and after 60 s of HF wet etching when deposited over the TiN surface etched using SO₂/O₂/He, SO₂ only, O₂ only, He only, and SO₂/O₂/He without RF bias power.

| Neutral layer thickness (nm) | Before HF | After HF |
|---|-----------|-----------|
| SO ₂ /O ₂ /He | 7.1 ± 0.4 | 0.0 ± 0.0 |
| SO ₂ only | 8.2 ± 0.5 | 0.5 ± 0.2 |
| O ₂ only | 9.2 ± 0.4 | 9.3 ± 0.5 |
| He only | 6.3 ± 0.6 | 6.5 ± 1.1 |
| SO ₂ /O ₂ /He zero bias | 7.0 ± 0.5 | 0.9 ± 0.2 |

17 February 2025 13:02:13

neutral layer deposition and HF wet etching have been conducted following the same procedure described in Sec. III B 3. The thickness measurement results are presented in Table VI. After SO₂ only and SO₂/O₂/He with zero bias, the neutral layer is almost completely removed after wet etching. As for the O₂ only and He only samples, no significant thickness variation is observed after HF.

Therefore, it is possible to conclude that, while oxygen alone highly oxidizes the TiN surface and increases its surface energy, it does not have a significant negative effect on the neutral layer adherence, thus allowing this layer to resist the HF wet etching step. The same is observed for the helium: based on the ellipsometry measurements, it does not seem to prevent the adherence of the neutral layer. Another parameter evaluated was the RF bias power, which does not seem to be the most significant parameter. Without RF bias, even though the TiN modified layer is less thick when compared to the same process with bias, the neutral layer is still almost completely removed, which means the SO₂/O₂/He plasma etching chemistry is not adapted to the chemoepitaxy application. This leads to the conclusion that the SO₂ molecule is the main one responsible for this recipe's inadequacy to this application: the SO₄²⁻ ions on the TiN surface probably react with the neutral layer's crosslinking agent, which prevents its complete crosslinking and allows the HF to pass through. The HF then removes the modified TiO₂/TiO_xS_y layer formed on the TiN surface, which reduces the neutral layer adherence to the TiN hard mask and allows its consequent lift-off.

E. Alternatives for the SOC etching step

In this part, we propose alternatives to replace the SOC etching step based on SO₂/O₂/He, which is not favorable to the neutral layer adherence. We have chosen to replace the SOC etching step instead of the trilayer etching for a couple of reasons. The first one is related to a higher freedom of choice, because while the trilayer etching must be anisotropic in order to correctly transfer the lithography patterns into the SOC layer, the SOC mandrel removal step has no constraint tied to the anisotropy, only to the selectivity regarding the SiN spacers. The second reason is that the SOC mandrel removal is the last step before the neutral layer deposition and, therefore, probably the one whose impact on the TiN surface is the most important.

Two different approaches have been explored: the first one is an oxygen only SOC etching, since it has been shown in Sec. III D 2 that oxygen does not have a negative effect on the neutral layer wetting capability. The second approach is a reductive SOC etching based on H₂/N₂. Both approaches are well-known SOC and resist stripping chemistries and their plasma parameters were taken from the already existing recipes used in other applications. The oxygen only etching is conducted on the ICP reactor with 200 sccm of O₂ during 30 s, with an RF power of 1320 W, a pressure of 10 mTorr, and zero RF bias. The H₂/N₂ reductive SOC etching, on the other hand, is conducted in a capacitively coupled plasma reactor due to H₂ not being available in the ICP reactor. The plasma parameters are H₂/N₂ 150/500 sccm, during 60 s with a pressure of 160 mTorr, RF 2 MHz power at zero and RF 27 MHz power at 1000 W.

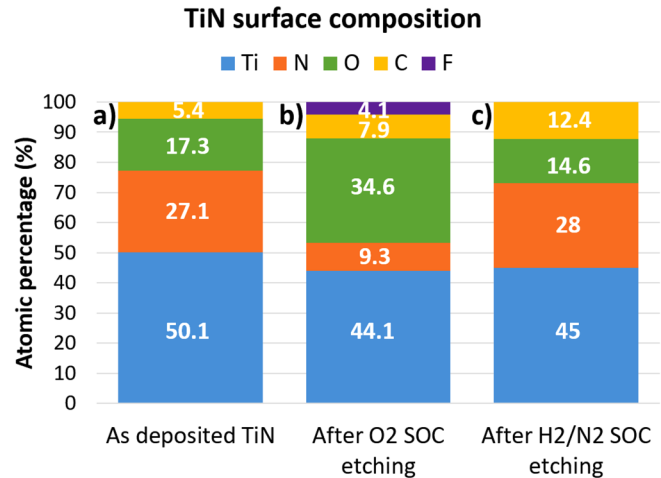


FIG. 9. TiN surface composition determined by *ex situ* XPS: (a) before etching; (b) after O₂ only SOC etching; and (c) after H₂/N₂ SOC etching.

1. Effect of the SOC etching alternatives on the TiN surface composition

The XPS results for both approaches are presented in Fig. 9, along with the results before etching for comparison purposes. For the oxygen only SOC etching [Fig. 9(b)], as expected, it is possible to observe a significant increase of about 17.3% for the oxygen percentage, characterized by an intensity increase in the TiO₂ peak. Consequently, an equivalent decrease of around 17.8% is observed for the nitrogen content, indicating a reduction of the TiN peak intensity. As for the titanium percentage, a decrease of 6% is observed, which is a combination of both TiO₂ peak intensity augmentation and TiN peak intensity reduction. As for the H₂/N₂ SOC etching [Fig. 9(c)], the slight decrease in Ti and O percentages is explained by the increase in the carbon contamination, which comes from the reactor's chamber walls and the air exposure between etching and XPS analysis. Therefore, no significant changes are observed for the TiN surface composition after etching using H₂/N₂.

17 February 2025 13:02:13

2. Contact angle and surface energy measurements

Contact angle measurements have also been conducted to obtain the surface energy of these samples after etching and the

TABLE VII. TiN surface energy before and after the alternative SOC etching approaches, calculated by contact angle measurements, as well as its dispersive and polar components.

| | Surface energy γ (mN/m) | Dispersive component γ_d (mN/m) | Polar component γ_p (mN/m) |
|--|--------------------------------|--|-----------------------------------|
| As deposited TiN | 43.8 | 37.3 | 6.5 |
| After O ₂ etching | 76.1 | 42.9 | 33.2 |
| After H ₂ /N ₂ etching | 54.2 | 47.3 | 6.9 |

results are presented in Table VII. For the oxygen only etching, the results obtained were similar to those seen in Secs. III C 2 for other oxidative chemistries: a significant increase in the surface energy and polar component after etching. As for the H₂/N₂ etching, it is important to notice that the polar component is similar to that of the as deposited TiN, which indicates a natural compatibility with the neutral layer.

3. Effect of the wet spacer removal step on the neutral layer adherence

Like in Secs. III B 3 and III C 3, the neutral layer deposition and HF wet etching have been conducted in order to verify the correct adherence of the neutral layer over the modified TiN surface after etching. Table VIII presents the thickness measurement results: for both SOC etching approaches, the neutral layer presents the same thickness before and after HF wet etching. The TiN + xNL surface for both approaches has also been verified by cross-sectional SEM and, as expected based on the results from Table VIII, both surfaces are smooth and do not present lift-off spots. Therefore, both approaches present a favorable surface for the neutral layer adherence.

4. Application to pattern wafers using the ACE chemoepitaxy flow

Finally, these SOC etching steps have been applied to pattern wafers following the complete ACE flow presented in Sec. II A. Figure 10 represents the results obtained after the BCP self-assembly step for the PS-*b*-PMMA block copolymer with 32 nm pitch. The PMMA phase has been removed through dry etching to enhance the contrast and facilitate the image capture. For both processes, we observe a great improvement compared to the first result presented in Fig. 3. The top-view SEM image after oxygen only etching [Fig. 10(a)] does not present lift-off spots, but it still presents very few BCP self-assembly defects, such as small dark spots and alignment defects. As for the H₂/N₂ SOC etching, Fig. 10(b) represents a 10 × 10 μm² (the largest measurement field the CD-SEM tool used can obtain) image without any type of alignment or lift-off defects, which translates to 0 def/100 μm².

Therefore, it is possible to conclude that the H₂/N₂ chemistry is the most adequate SOC etching approach for the chemoepitaxy ACE process flow due to its capacity to conserve the surface properties of the as deposited TiN, such as its surface energy and composition. As for the oxygen only approach, it does not present lift-off spots, but it still presents some alignment defects. Further experiments are currently ongoing in order to understand the origin of these defects.

TABLE VIII. Neutral layer thickness measured by ellipsometry before and after HF wet etching when deposited over the TiN surface after etching using O₂ only and H₂/N₂.

| Neutral layer thickness (nm) | After HF | |
|--|-----------------------|-------------|
| | Before HF wet etching | wet etching |
| O ₂ only etching | 6.7 ± 0.3 | 6.8 ± 0.3 |
| H ₂ /N ₂ etching | 6.9 ± 0.1 | 7.0 ± 0.1 |

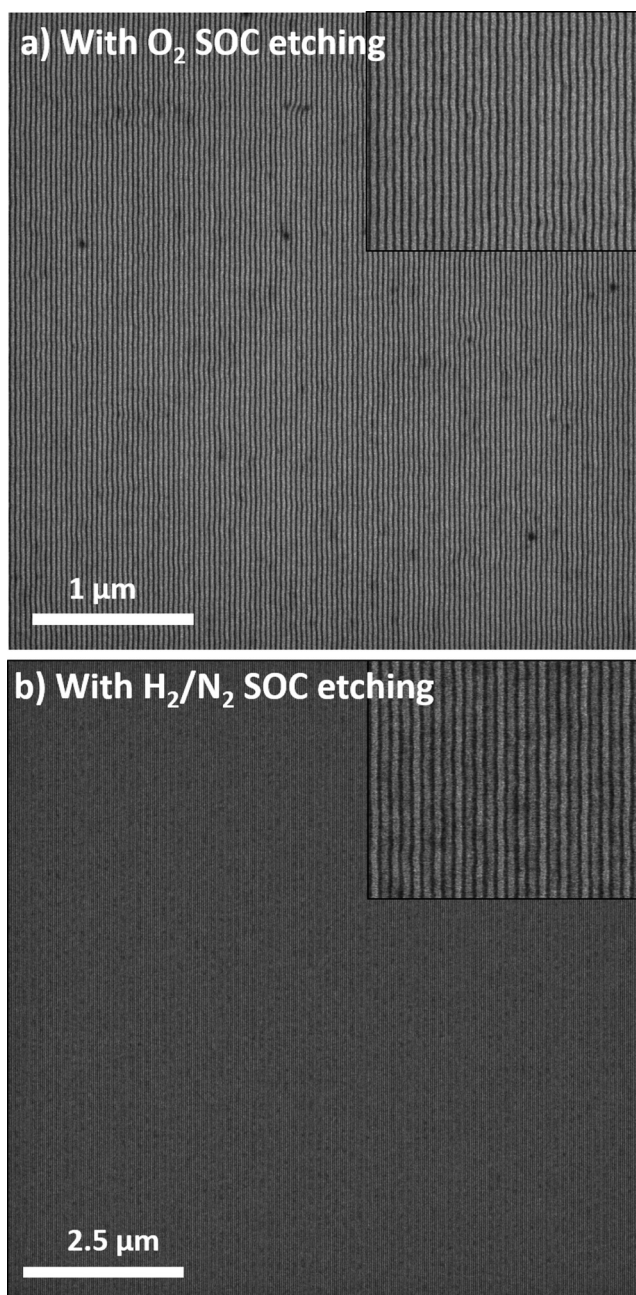


FIG. 10. Top-view SEM images of the PS-*b*-PMMA block copolymer with pitch 32 nm aligned by the ACE flow using (a) oxygen only SOC etching and (b) H₂/N₂ SOC etching. Both images correspond to a lithography pitch of 128 nm and present a zoomed view to highlight the good alignment obtained.

17 February 2025 13:02:13

IV. SUMMARY AND CONCLUSIONS

In this paper, we have studied the effects of the different etching steps present on the (ACE chemoepitaxy process flow on

the surface properties (composition and surface energy) of the titanium nitride hard mask. The goal was to evaluate the hard mask's capability to ensure the correct adherence of the PS-*r*-PMMA neutral layer after the different etching and deposition steps. By studying the effect of each etching step on the TiN blanket wafers, we observed that all of them induced significant surface energy and composition modifications when compared to the pristine TiN hard mask. Next, to verify the adherence of the neutral layer to the TiN surface modified by the different etching steps, the neutral layer thickness was measured before and after HF wet etching. Ellipsometry measurements showed that the neutral layer is completely removed for the samples after trilayer etching and SOC etching, which were both based on SO₂/O₂/He. This led to the conclusion that the TiN surface after SO₂/O₂/He plasma is not favorable to the neutral layer adherence and, as a result, this layer is not able to resist the HF wet etching. Further investigation showed that the SO₂ molecule is the main responsible for the lift-off.

Two different alternatives for the SOC etching were then explored: O₂ and H₂/N₂. The oxygen only approach presented surface energy and composition modifications similar to the ones observed before for the other SOC etching step investigated: strong oxidation of the TiN surface and increase in the surface energy's polar component. As for the H₂/N₂ approach, the surface composition and surface energy's polar component were similar to the ones measured for the pristine TiN surface. For both SOC etching approaches, the neutral layer presented the same thickness before and after HF wet etching. Therefore, both approaches presented a favorable surface for the neutral layer adherence. Finally, when applying these SOC etching alternatives to pattern wafers, the CD-SEM image after oxygen only SOC etching presented very few self-assembly and alignment defects of the BCP. The H₂/N₂ SOC etching, on the other hand, did not present any type of defects, which translates to 0 def/100 μm² and leads to the conclusion that the H₂/N₂ chemistry is the most adequate SOC etching approach for the chemoepitaxy ACE process flow due to its capacity to conserve the surface properties of the as deposited TiN, such as its surface energy and composition.

ACKNOWLEDGMENTS

The authors would like to thank C. Navarro from Arkema and K. Sakavuyi from Brewer Science Inc. for supplying the different

polymeric materials. This work has been financed by the REX-7 project (Grant Agreement No. DOS0075457/00) from the region Auvergne-Rhône Alpes, the DiSABlock chair of excellence of the Grenoble Nanoscience Foundation, and the European ECSEL project MADEin4 (Grant Agreement No. 826589). It has also been supported by the French National Research Agency (ANR) within the IMPACT program, under Contract No. ANR-10-EQPX-33. The authors also thank SCREEN and Applied Materials for their continued support.

DATA AVAILABILITY

The data that support the findings of this study are available within the article and from the corresponding author upon reasonable request.

REFERENCES

- ¹G. E. Moore, *Electronics* **38**, 114 (1965). [reprinted in IEEE Solid-State Circuits Society Newsletter **11**, 33–35 (2006)].
- ²G. E. Moore, *IEEE IEDM* **21**, 11 (1975).
- ³M. P. Stoykovich and P. F. Nealey, *Mater. Today* **9**, 9 (2006).
- ⁴N. Posseme, *Plasma Etching Process for CMOS Devices Realization* (Elsevier, Amsterdam, 2017).
- ⁵G. Claveau, *Etude D'une Lithographie Ligne/Espace Innovante par Auto-Assemblage Dirigé D'un Copolymère à Blocs Pour la Réalisation de Dispositifs CMOS Sub-20 nm* (Université Grenoble Alpes, Grenoble, 2017) (in French).
- ⁶M. Argoud *et al.*, *Proc. SPIE* **9049**, 904929 (2014).
- ⁷S.-J. Jeong, J. Y. Kim, B. H. Kim, H.-S. Moon, and S. O. Kim, *Mater. Today* **16**, 468 (2013).
- ⁸H. Tsai *et al.*, *ACS Nano* **8**, 5 (2014).
- ⁹G. Claveau *et al.*, *J. Micro/Nanolithogr., MEMS, MOEMS* **15**, 031604 (2016).
- ¹⁰C.-C. Liu, E. Han, M. S. Onses, C. J. Thode, S. Ji, P. Gopalan, and P. F. Nealey, *Macromolecules* **44**, 1876 (2011).
- ¹¹J. Kim *et al.*, *J. Photopolym. Sci. Technol.* **26**, 573 (2013).
- ¹²A. Paquet *et al.*, *Proc. SPIE* **10958**, 109580M (2019).
- ¹³G. J. Rademaker *et al.*, *Proc. SPIE* **11326**, 11326OZ (2020).
- ¹⁴D. K. Owens and R. C. Wendt, *J. Appl. Polym. Sci.* **13**, 8 (1969).
- ¹⁵D. Gonbeau, C. Guimon, G. Pfister-Guillouzo, A. Lévassieur, G. Meunier, and R. Dormoy, *Surf. Sci.* **254**, 1 (1991).
- ¹⁶S. Oktay, Z. Kahraman, M. Urgen, and K. Kazmanli, *Appl. Surf. Sci.* **328**, 255 (2015).
- ¹⁷C. D. Wagner and J. A. Taylor, *J. Electron Spectrosc.* **28**, 2 (1982).
- ¹⁸N. Tjitra Salim, M. Yamada, H. Nakano, K. Shima, H. Isago, and M. Fukumoto, *Surf. Coat. Technol.* **206**, 366 (2011).